Journal of Materials Chemistry C

ROYAL SOCIETY OF CHEMISTRY

PAPER

View Article Online
View Journal | View Issue

Check for updates

Cite this: J. Mater. Chem. C, 2021, 9, 1429

2D layered metal-halide perovskite/oxide semiconductor-based broadband optoelectronic synaptic transistors with long-term visual memory†

Youngjun Park, Min-Kyu Kim and Jang-Sik Lee *

Received 6th September 2020,
Accepted 22nd December 2020

DOI: 10.1039/d0tc04250a

rsc.li/materials-c

To implement neuromorphic visual systems that can perceive and memorize optical information, it is essential to realize the artificial synapses that respond to optical signals. Organic–inorganic halide perovskites (OIHPs) have been considered as optically modulated synapses due to high absorption coefficient and long charge-carrier lifetime. However, it is difficult to store the optical information because photo-excited carriers recombine after removal of illumination. Here, we combine an OIHP with indium zinc tin oxide (IZTO) to implement artificial synapses that can perceive and memorize optical information for long-term storage in neuromorphic visual systems. The transparent IZTO on OIHP allows optical signal absorption by the OIHP and protects it from atmosphere exposure. Excellent optical absorption of OIHP leads to generation of photo-excited carriers, and the band alignment between IZTO and OIHP facilitates the spatial separation of photo-excited carriers that serves as the basis of optically-meditated charge trapping; these characteristics enable nonvolatile change in conductance. Optical synapses show potentiation/depression under multiple wavelengths with a large dynamic range of $\sim 10^4$, which is significantly advantageous for recognition accuracy in artificial neural networks. These results demonstrate the feasibility of OIHP-based optical synapses for neuromorphic visual systems.

Published on 05 2021. Downloaded on 31.01.2026 06:16:23.

Introduction

Vision is the main sense by which humans perceive their environment.[1,2] Optical information sensed by the retina is transmitted and interpreted by neural networks.[3] In neural networks, synapses are the basic units that transmit, process, and memorize visual information.[3] These processes can be achieved by synaptic plasticity, which is a change of connection strength of a synapse in response to repeated stimulation, in this case by light signals.[4] Therefore, the implementation of neuromorphic visual systems requires emulation of this synaptic plasticity in response to the optical stimuli. For this purpose, artificial synapses for vision perception have been designed by connecting a photodetector to a memory device,[5–7] but this physical separation of the optical sensing and memory requires complex integrated circuits that cause low efficiency and high power consumption. The solution to this problem is to develop a device that can perform detection and synaptic behaviors simultaneously.

To implement such artificial synapses, various materials have been evaluated using graphene, quantum dots, transition metal dichalcogenides, and organic–inorganic halide perovskites (OIHPs).[8–12] Especially, OIHPs have superior optical properties such as high optical absorption coefficient, long carrier diffusion length, and low exciton binding energy, and therefore have been considered as promising candidates for artificial synapses.[8,13–18] However, OIHPs are easily degraded by air and moisture.[19,20] Two-dimensional (2D) layered OIHPs have been evaluated to overcome these problems.[21–23] 2D layered OIHPs can be regarded as derivatives of 3D OIHPs by replacing a small methylammonium cation (MA^+) with a large ammonium cation such as butylammonium (BA^+) or phenylethylammonium (PEA^+).[22,24] These OIHPs are stable in ambient air because the large cations can impede moisture infiltration.[22] Also, the optical and electrical properties of 2D layered OIHPs can be easily modulated by modifying their compositions.[23,25] However, although OIHPs have superior optical properties, they show only temporary change in conductance under illumination; and after removal of the illumination, the changed conductance decays rapidly due to recombination of photo-excited carriers.[26,27] These properties impede applications of OIHPs as artificial synapses that require combined memory and learning functions. Thus, to store the information about optical stimulation, OIHPs

Materials Science and Engineering, Pohang University of Science and Technology (POSTECH), Pohang 37673, Korea. E-mail: jangsik@postech.ac.kr; Tel: +82 54-279-2153

† Electronic supplementary information (ESI) available. See DOI: 10.1039/d0tc04250a

Published on 05 2021. Downloaded on 31.01.2026 06:16:23.

have been developed as artificial synapses by introducing integrated structures with other materials such as pentacene with a floating-gate structure or Si nanomembrane.[13,18,28,29] Synaptic behaviors in these devices result from the movement and trapping of photo-excited carriers between perovskite and channel layer. Also, to apply the artificial synapses to artificial neural networks (ANNs), the synapses should have large dynamic range (*i.e.*, the ratio of maximum conductance to minimum conductance) and linear/symmetric synaptic weight updates. These properties would enable the implementation of ANNs with high recognition accuracy,[30,31] so to obtain these properties, the development of materials and device structures for artificial synapses is required.

In this study, we develop an optical synapse that combines 2D layered OIHP of $(C_4H_9NH_3)_2PbBr_4$ (BA_2PbBr_4, BA = butylammonium) with transparent oxide semiconductor of indium zinc tin oxide (IZTO). The use of IZTO on OIHP enables implementation of bottom-gate structure. In this optical synapse, the OIHP shows strong optical absorption, and therefore can be efficiently stimulated by optical spikes. The band alignment between IZTO and 2D layered OIHP can lead to the effective spatial separation of photo-excited carriers that serves as the basis of optically meditated charge trapping, which enables nonvolatile conductance change. The device shows potentiation/depression characteristics with a large dynamic range of $\sim 10^4$. The large dynamic range can allow a large number of distinct synaptic weight states, which can improve the recognition accuracy in ANNs.[31] Also, the large dynamic range can increase mapping capability of synaptic weights in algorithms that normalize synaptic weights to a range between 0 and 1.[30] Symmetry and linearity of potentiation/depression characteristics are improved by controlling depression pulses. In a simulation using these properties, ANNs that use these optical synapses achieve 80% recognition accuracy of handwritten digits. These results demonstrate the feasibility of an optical synapse based on 2D layered OIHP and provide a promising resource for development of neuromorphic visual systems.

Experimental section

Materials

Lead bromide ($PbBr_2$, 98% purity) was purchased from Sigma-Aldrich. *n*-Butylammonium bromide (BABr) was purchased from GreatCell Solar. Si wafers with a 300 nm-thick thermally-grown SiO_2 were used as the substrate.

Device fabrication

SiO_2/Si substrate was cleaned by sequential ultrasonication in acetone, ethanol, and distilled water for 10 min each. The OIHP layer was formed by sequential vapor deposition. First, $PbBr_2$ thin film was deposited on the substrate by thermal evaporation using $PbBr_2$ powder. Then, the $PbBr_2$ film deposited on the substrate was transferred to a glove box. To transform the $PbBr_2$ to BA_2PbBr_4, $PbBr_2$ film was exposed to BABr vapor that was prepared by heating the BABr powder (3 mg) sprinkled on a glass Petri dish. BaBr molecules were intercalated into $PbBr_2$ frames during exposure to BABr vapor; consequently, the $PbBr_2$ layer was transformed to BA_2PbBr_4 with layered structure. This treatment was performed at 150 °C for 3 h on a hot plate. Then IZTO film was deposited on the OIHP layer by co-sputtering from ITO and ZnO targets. The RF power of 100 W was used for the ZnO target, and DC power of 100 W was used for the ITO target. Sputtering was performed with the gas flow of Ar/O_2 (10/4 sccm) at the deposition pressure of 5 mTorr. Finally, Al source and drain electrodes of 100 nm thickness were deposited on the IZTO layer by e-beam evaporation.

Characterization

All electrical characteristics of the optical synapse were measured using a semiconductor parameter analyser (4200A-SCS, Keithley) in the probe station. The crystal structures of $PbBr_2$ and 2D layered OIHP were investigated using X-ray diffraction (XRD, D/MAX-2500, Rigaku) with Cu Kα radiation. The optical responses were measured by applying monochromatic light from a xenon lamp under ambient conditions with a light source (Model 71SI00059, Newport). Memorization of letter 'N' images by the optical synapse array was performed by optical spike input to each device in a 5 × 5 synapse array.

Results and discussion

A human perceives optical information *via* the retina (Fig. 1a). Nerve cells in a retina transform optical information to neural impulses, which are transmitted along the optic nerve to the visual cortex in the brain.[3] The visual cortex consists of a large number of neurons and synapses that can process and memorize information.[3,32] We emulated these properties of a visual system by implementing optical synapses composed of 2D layered BA_2PbBr_4 and IZTO. The BA_2PbBr_4 was composed of an inorganic layer of $[PbBr_6]^{4-}$ octahedra sandwiched between two organic $[C_4H_9NH_3]^+$ layers (Fig. 1b). The BA_2PbBr_4 was formed by sequential vapor deposition of $PbBr_2$ and BABr on SiO_2/Si substrate (Fig. 1c).[33] This process could form an OIHP layer that has uniform surface coverage and controllable thickness.[34,35] A $PbBr_2$ layer was first deposited on the substrate by thermal evaporation. Then BABr was deposited on the $PbBr_2$ layer to form the BA_2PbBr_4. BaBr molecules became intercalated into the $PbBr_2$ frames during this process, then $PbBr_2$ was transformed to BA_2PbBr_4. To confirm the formation of BA_2PbBr_4 OIHP, we analyzed the XRD patterns. The XRD patterns of BA_2PbBr_4 showed (00*l*) diffraction peaks, which indicated the preferential orientations along *c*-axis (Fig. 1d).[33,36] To confirm whether sputtering of IZTO affects the quality of the OIHP, we analyzed the XRD patterns of BA_2PbBr_4 after the deposition of IZTO. Diffraction peaks assigned to (002), (004), (006), (008), and (0010) planes were observed (Fig. S1, ESI†); this result is consistent with the peaks observed on the BA_2PbBr_4 film before deposition of IZTO. These results indicated that the sputtering process did not noticeably affect the OIHP film.

 This journal is © The Royal Society of Chemistry 2021

Published on 05 2021. Downloaded on 31.01.2026 06:16:23.

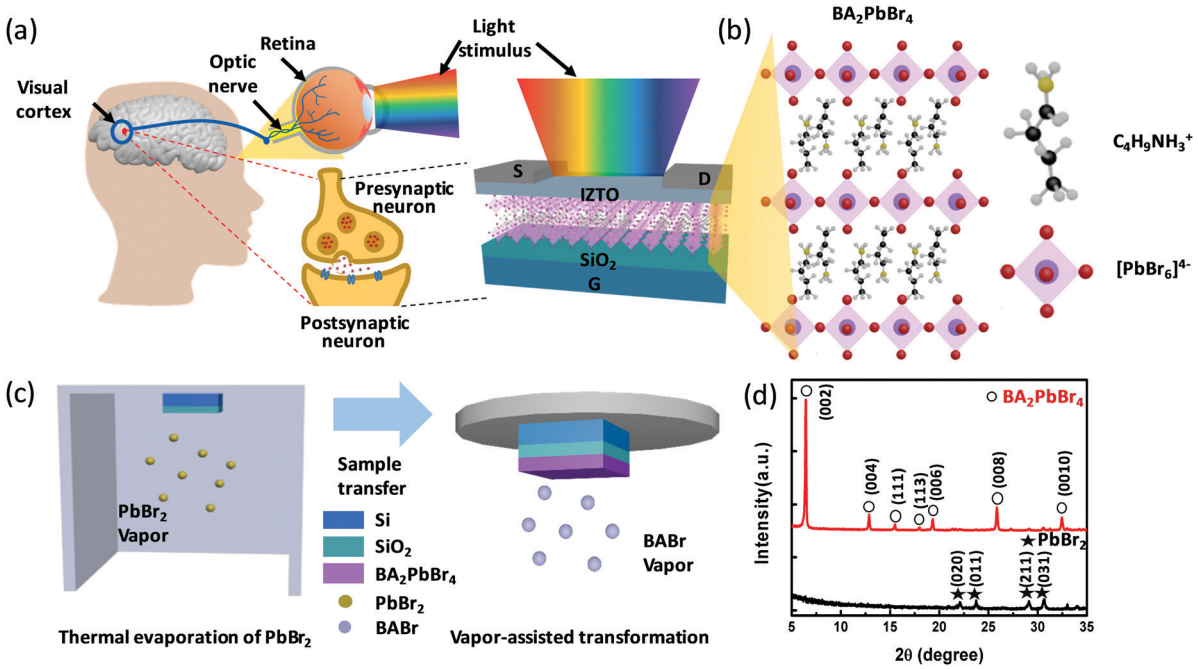

Fig. 1 (a) Schematic illustrations of human visual system and optical synapse composed of 2D layered OIHP with IZTO. Al is used for source (S) and drain (D) electrodes; Si is used as the gate electrode (G). (b) Schematic structure of BA_2PbBr_4 (atom colors: Pb = blue; Br = red; C = black; N = yellow; H = grey). (c) Schematic illustrations of procedures to deposit the 2D layered OIHP using the sequential vapor deposition process. $PbBr_2$ film is deposited by thermal evaporation, then this $PbBr_2$ film is exposed to BaBr vapor to convert $PbBr_2$ to BA_2PbBr_4. (d) XRD patterns of $PbBr_2$ and BA_2PbBr_4.

The transfer characteristics of the device were measured by applying gate voltage V_G to the Si gate electrode under a drain voltage V_D of 5 V. When an optical pulse with a wavelength $\lambda = 365$ nm and intensity $L_I = 100$ μW cm^{-2} was irradiated to the device for 30 s, drain current I_D abruptly increased and the threshold voltage shifted in the negative direction. (Fig. 2a). The threshold voltage was changed more in the device that combined IZTO with 2D layered OIHP than in the device that used only IZTO (Fig. S2, ESI†). These results indicated that electron–hole pairs generated by light illumination in the OIHP layer could

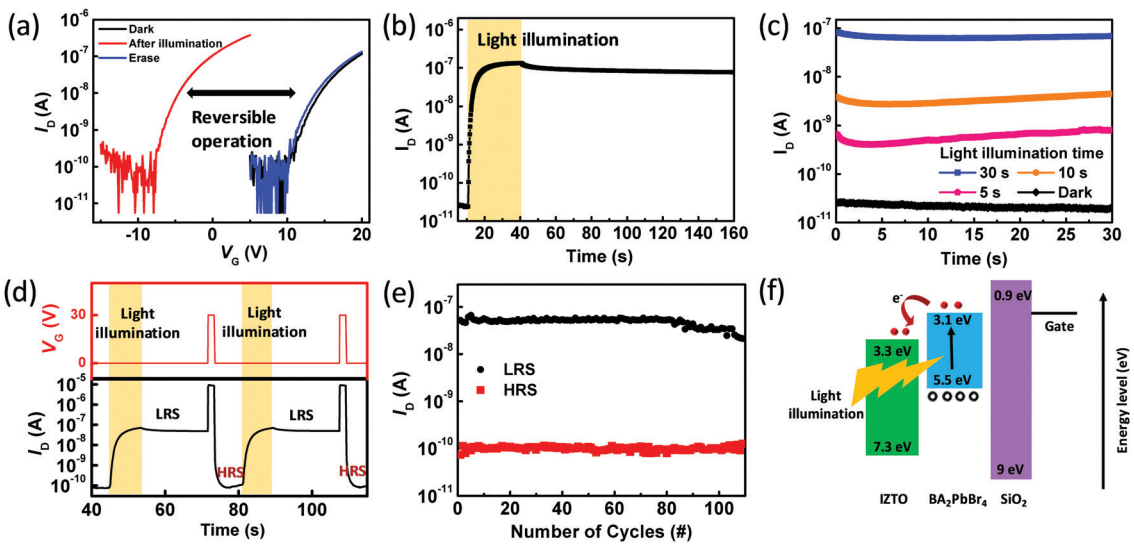

Fig. 2 (a) Transfer characteristics of the device in 'dark', 'after illumination', and 'erase' operation. Transfer characteristic of 'after illumination' state is measured 30 s after application of optical pulse (365 nm, 100 μW cm^{-2}, 30 s) under V_G sweep from −15 to 5 V. Transfer characteristic of 'erase' state is measured after applying a positive V_G pulse (30 V, 2 s) under V_G sweep from 5 to 20 V. (b) Retention property after light illumination for 30 s. (c) Change of I_D with different durations of illumination (5 s, 10 s, 30 s) and without illumination. (d) The resistance change of the device by applying optical spikes (365 nm, 100 μW cm^{-2}, 10 s) and applying positive V_G (30 V, 2 s). (e) Change of I_D between LRS and HRS for 110 cycles. (f) Schematic illustration of band diagram of the IZTO/2D layered OIHP device under illumination.

Published on 05 2021. Downloaded on 31.01.2026 06:16:23.

contribute to the device operation. Transfer curve that shifted in the negative direction returned to its initial state after the application of a positive V_G pulse (30 V, 2 s). To further quantify the effect of illumination, the device was exposed to light (365 nm, 100 μW cm^{-2}) for 30 s, without applying V_G (*i.e.*, V_G = 0 V). The I_D increased abruptly from high-resistance state (HRS) to low-resistance state (LRS) during illumination; and the ratio of the current values of the two states was $\sim 10^4$ (Fig. 2b). The device remained in LRS for 10^4 s after the illumination ceased (Fig. S3, ESI†). The long retention time may be related to optically-meditated charge trapping, so it is important to understand charge trapping mechanism and trap energy levels. The trap depth can be calculated from attempt-to-escape frequencies and trap density of states obtained by thermal admittance spectroscopy measurement.[37–39] Among them, the attempt-to-escape frequency can be obtained by temperature-dependent capacitance-frequency measurement.[38,40] Deep-level traps may be formed for long retention time. 2D layered OIHPs are known to have deep level defects.[41,42] Butylammonium-based 2D layered OIHP has deep level defects with a defect activation energy of 0.398 eV, which is higher than that of 3D perovskite (0.075 eV).[42] In our device, 2D layered OIHP was used for optical signal absorption and the formation of deep traps in the 2D layered OIHP may enable long retention time. Also, we implemented four distinct resistance states by controlling light illumination time (Fig. 2c). These results demonstrated that the device showed the feasibility of multilevel data storage by modulating the illumination time. In addition, the device showed consecutive resistance change between HRS and LRS during repeated application of pulses. The change of resistance from HRS to LRS was achieved by an optical pulse (365 nm, 100 μW cm^{-2}, 10 s). The return to HRS from LRS was implemented by applying a V_G pulse (30 V, 2 s) (Fig. 2d). The 2D layered OIHP-based device was switched stably between HRS and LRS for 110 cycles (Fig. 2e). To confirm the stability, the device was kept in ambient air and transfer characteristics were measured. The device was operated stably without degradation after 14 days (Fig. S4, ESI†). There are several possible mechanisms for device operation in three-terminal devices such as ion migration and charge carrier transport. OIHP film includes several ions such as $CH_3NH_3^+$, Pb^{2+}, and halides.[43] In 3D OIHP, halide ions can move easily because they have a low ionic migration barrier.[44,45] However, in 2D OIHP, ion migration is suppressed because long-chain organic cations can act as a barrier that prevents the ion migration.[46,47] Also, ion migration in the OIHP is observed when voltage is applied and affects the electrical properties of device.[48,49] However, the fabricated device did not require the voltage to change the resistance from HRS to LRS. In contrast, movement of photo-excited carriers can affect the change of resistance state of device. The change of resistance state with optical signal may be a result of the photogating effect caused by photo-excited carriers.[50] The photogating effect has been reported in heterostructured devices that combine OIHP with oxide semiconductor, organic semiconductor, or graphene.[12,13,50–53] During light illumination, electron–hole pairs were generated in the 2D OIHP layer (Fig. 2f). The photo-excited carriers could be effectively dissociated by the built-in field that was induced by a bending of the energy band. The photo-excited electrons were transferred from OIHP layer to IZTO layer, whereas the photo-excited holes remained behind in OIHP layer. These holes could induce photogating effect and consequently increase current by capacitive coupling.[50] The number of remaining holes could be reduced by recombination under positive V_G, and thereby overcome the barrier to prompt electron injection from IZTO to OIHP layer, so the increased I_D could return to its initial state.

Synapses are responsible for signal transmission, memory, and learning functions in a brain.[54] Biological synapses are located between presynaptic and postsynaptic neurons. The synapses perform their functions by adapting their connection strength, which is called 'synaptic plasticity'.[55,56] Synaptic plasticity can be classified into short-term plasticity (STP) and long-term plasticity (LTP).[57,58] STP is a temporary change in synaptic weight that lasts a few seconds to minutes; LTP is a permanent change in synaptic weight that lasts days to years.[58] We emulated synaptic plasticity by using the device. STP was emulated by applying an optical pulse with a short pulse duration that was insufficient to induce a permanent change of current. When optical pulses (365 nm, 100 μW cm^{-2}) with a duration of 50 ms were applied, the I_D increased, then decayed after the applied pulses ended (Fig. 3a). Also, we emulated paired-pulse facilitation (PPF) using the device. PPF is the phenomenon in which a second presynaptic spike causes a larger postsynaptic current than the first spike does.[59] The degree of increase in the second postsynaptic current decreases with an increase in the time interval Δt between the two spikes. A biological synapse exploits PPF to recognize and decode temporal information.[60] To emulate this characteristic, we applied two consecutive optical pulses (365 nm, 100 μW cm^{-2}, 200 ms) with Δt = 400 ms. The first spike yielded an increased amplitude A_1 of I_D, and the second spike yielded a further increased amplitude A_2 (Fig. 3b). Also, we investigated the change of PPF value by adjusting Δt between two pulses. The PPF index was defined as a ratio between A_2 and A_1 ($A_2/A_1 \times 100\%$).[60] The PPF index was 55% at Δt = 100 ms, and decreased to 21% at Δt = 2 s (Fig. 3c). The decay in PPF index was described using a double-exponential function,[61,62]

$$\text{PPF index} = 1 + C_1 \times \exp\left(-\frac{\Delta t}{\tau_1}\right) + C_2 \times \exp\left(-\frac{\Delta t}{\tau_2}\right)$$

where C_1 and C_2 are initial facilitation magnitudes, and τ_1 and τ_2 are relaxation time constants. Curve fitting yielded τ_1 = 45 ms and τ_2 = 2.2 s. The change of PPF index with two distinct phases is similar to the response of a biological synapse.[59] LTP could be obtained by applying a consecutive pulse long enough to induce permanent change of current. When optical pulses (365 nm, 100 μW cm^{-2}, 1 s) were applied, I_D increased and was maintained without returning to its initial state (Fig. 3d). Also, the magnitude of the change in I_D could be controlled by application of different numbers of optical pulses (N = 5, 10, 20, 50) (Fig. 3e). As N was increased, I_D after pulse application gradually increased. The change in I_D could also be controlled by adjusting λ of the applied optical spikes. The changes in current with wavelengths have been reported in OIHP-based synapse devices and photodetectors.[14,18,50,63] To confirm this characteristic, we

 This journal is © The Royal Society of Chemistry 2021

Published on 05 2021. Downloaded on 31.01.2026 06:16:23.

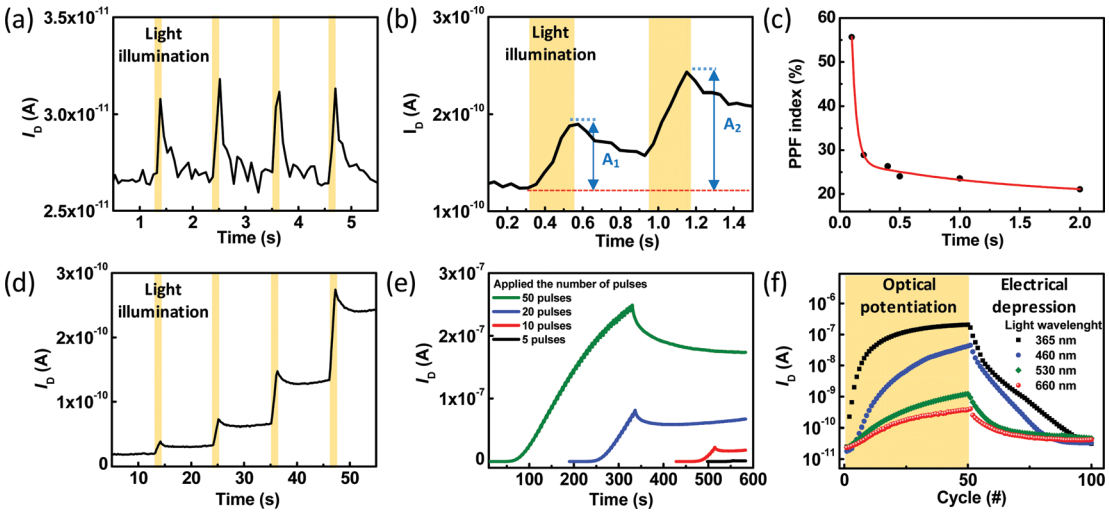

Fig. 3 (a) STP characteristics with four consecutive optical spikes (365 nm, 100 μW cm^{-2}, 50 ms). (b) Change of I_D after two consecutive optical pulses (365 nm, 100 μW cm^{-2}, 200 ms) separated by Δt = 400 ms. A_1 is the change of I_D after the first spike; A_2 is the change of I_D after the second spike. (c) Decrease in PPF = $A_2/A_1 \times 100\%$ with increase in time interval Δt between two optical spikes. (d) LTP characteristics by four consecutive optical spikes (365 nm, 100 μW cm^{-2}, 1 s) (e) Change of I_D by the number of applied optical spikes (N = 5, 10, 20, 50). (f) Potentiation and depression characteristics of the ITZO/2D layered OIHP device. 50 optical spikes (100 μW cm^{-2}, 1 s) with different wavelengths were applied for potentiation process and 50 positive V_G pulses (20 V, 2 s) were applied for depression process.

applied red (630 nm), green (530 nm), blue (460 nm), or UV (365 nm) optical spikes (100 μW cm^{-2}, 200 s) to induce LTP (Fig. S5, ESI†). All applied spikes could induce LTP characteristics in the device. As λ was decreased, the change in I_D increased. These changes can be related to strong absorption of OIHP in the short wavelength region.[18] Based on this effect of λ on LTP characteristics, we measured the potentiation and depression characteristics. Fifty consecutive optical spikes (100 μW cm^{-2}, 1 s) with different λ were applied to the device to emulate potentiation, whereas fifty consecutive positive V_G spikes (20 V, 2 s) were applied to emulate depression (Fig. 3f). When optical spikes with λ = 660 nm were applied, I_D gradually increased from 10 pA and 300 pA, and I_D returned to its initial state after positive V_G spikes were applied. When optical spikes with λ = 365 nm were used, the change of I_D for potentiation and depression increased significantly and achieved a large dynamic range of $\sim 10^4$. It is known that a dynamic range of artificial synapse should be sufficiently large for high recognition accuracy in ANNs.[64] Also, a large dynamic range permits a large number of conductance states with well separated states; these characteristics improve tolerance to write noise and to device-to-device variations.[31] Furthermore, a large dynamic range can improve mapping capability of synaptic weights in algorithms that normalize synaptic weights to a range between 0 and 1.[30] The dynamic range of $\sim 10^4$ is advantageous for application to neuromorphic computing. To confirm the effect of frequency on potentiation characteristics, we applied the ten consecutive optical spikes (365 nm, 100 μW cm^{-2}, 1 s) with different frequencies (0.83 Hz, 0.5 Hz, 0.33 Hz) (Fig. S6, ESI†). The I_D increased as the frequencies of applied optical spikes increased. These results indicated that the potentiation characteristics could be controlled by the frequency of applied optical spikes.

The goal in developing artificial synapses is to apply the devices to practical ANNs. The introduction of artificial synapses with weight-update characteristics can accelerate the training process and reduce power consumption in ANNs.[65] Simulation can easily confirm the possibility of the fabricated device in practical application. We performed simulation to confirm the applicability of the fabricated artificial synapses in ANNs. To investigate the learning capability of the artificial synapse driven by optical spikes, we simulated the recognition accuracy in ANNs. The simulation was conducted using a multilayer perceptron neural network with 400 input neurons, 100 hidden neurons, and 10 output neurons (Fig. 4a).[64,66] The Modified National Institute of Standard and Technology (MNIST) data set was used for the simulation. The multilayer perceptron algorithm was used in simulations with our experimental results of the optical synapse, including dynamic range, number of states, and linearity from the fitting result of potentiation and depression. Potentiation was performed by applying fifty optical spikes (365 nm, 100 μW cm^{-2}, 1 s). To improve the linearity for synaptic weight update, electrical pulses with incremental amplitudes were used for depression. Fifty consecutive pulses with amplitudes of V_G from 10 V to 29.6 V in increments of 0.4 V were applied to control the depression process (Fig. S7, ESI†). We compared recognition accuracy of depression processes with controlled V_G pulses and those with fifty consecutive identical V_G pulses (20 V, 2 s). In the simulation, recognition accuracy was 45% for identical-pulse condition and 80% for controlled-pulse condition (Fig. 4b). These results indicated that this optical synapse was applicable in ANNs for neuromorphic systems, and that recognition accuracy could be increased by controlling the potentiation/depression characteristics. We also emulated the functions of human visual memory that used the optical information sensing and memorizing capabilities of the optical synapse. The simulation used the conductance change under illumination of IZTO/2D layered OIHP (Fig. S8a, ESI†). To compare the

Published on 05 2021. Downloaded on 31.01.2026 06:16:23.

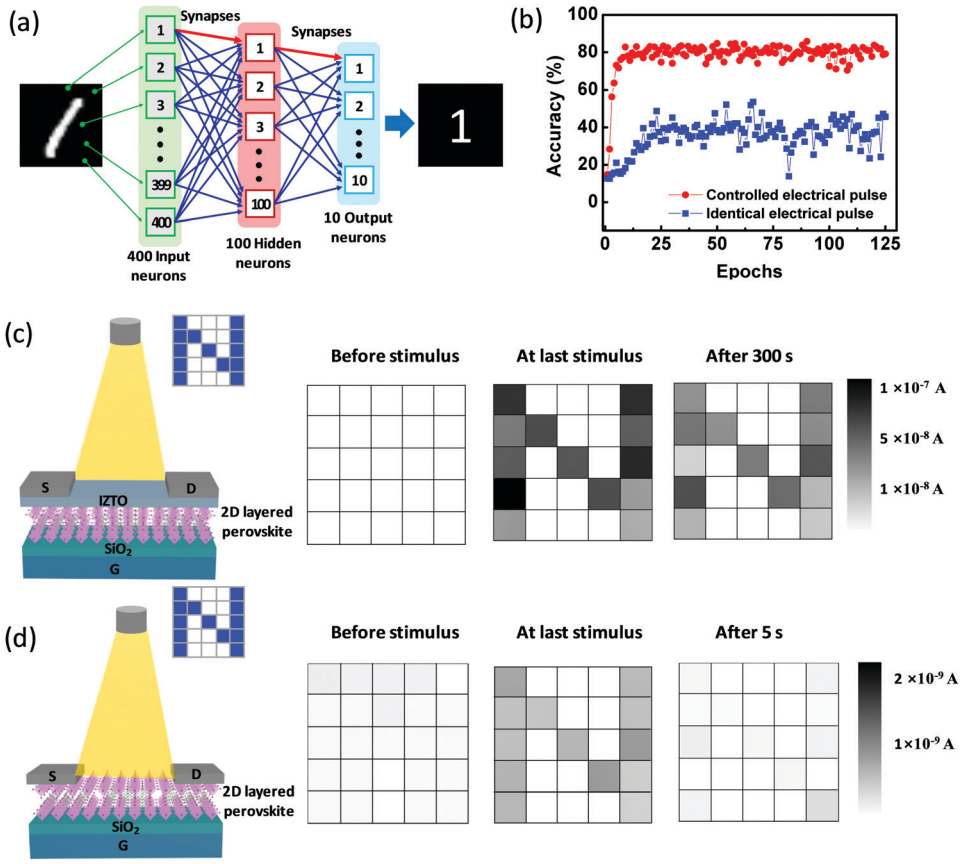

Fig. 4 (a) Schematic illustration of multilayer neural network composed of 400 input neurons, 100 hidden neurons, and 10 output neurons. (b) The recognition accuracy of artificial neural networks based on the artificial synapses that use IZTO/2D layered OIHP device for 125 epochs under identical and controlled pulse condition. (c) Current response before stimulus, at the last stimulus, and 300 s after last stimulus by inputting the optical stimuli with image of letter of "N" consisting of 5 × 5 pixels of IZTO/2D layered OIHP optical synapses and (d) current response before stimulus, at the last stimulus, and after 5 s of 2D layered OIHP device without IZTO.

possibility of human visual memory emulation, we also considered a device that used only 2D layered OIHP without IZTO (Fig. S8b, ESI†). Twenty-five devices were chosen to recognize and memorize the input image of letter "N" consisting of 5 × 5 pixel array. Before the optical stimuli were applied, all devices had low conductance because they were in the HRS. Each device was stimulated by application of optical pulses (365 nm, 100 μW cm^{-2}, 30 s), followed by decay measurement of postsynaptic current at 5 V for 60 s. The input image of letter "N" was recognized on all devices as a result of contrast in postsynaptic current. The IZTO/2D layered OIHP device showed reliable memorization for 300 s (Fig. 4c), whereas the 2D layered OIHP forgot the information after 5 s (Fig. 4d). These results indicated that integrated optical information sensing and memorizing capabilities of the IZTO/2D layered OIHP enabled mimicry of human visual memory.

Conclusions

We investigated an optical synapse that used a 2D layered OIHP (BA_2PbBr_4) and an amorphous oxide semiconductor (IZTO). The band alignment between IZTO and 2D layered OIHP could induce effective spatial separation of photo-excited carriers; this separation was the basis of optically-meditated charge trapping, and this trapping enabled control of conductance under illumination. The conductance increased by applying optical spikes, then returned to its initial state by applying electrical pulses. The device showed long-term potentiation and depression characteristics with a large dynamic range of $\sim 10^4$, which allowed a large number of distinct synaptic states that could improve the recognition accuracy in the neuromorphic system. We confirmed the applicability of the optical synapses to ANNs by simulation of recognition accuracy. These results demonstrated the feasibility of an optical synapse based on 2D layered OIHP. We believe that this work can provide a promising route to development of neuromorphic visual systems.

Author contributions

J.-S. L. conceived and directed the research. J.-S. L. and Y. P. designed and planned the experiment. Y. P. performed the experiment and acquired the data. J.-S. L., Y. P., and M.-K. K analyzed data. J.-S. L. and Y. P. wrote the manuscript.

 This journal is © The Royal Society of Chemistry 2021

Published on 05 2021. Downloaded on 31.01.2026 06:16:23.

Conflicts of interest

There are no conflicts to declare.

Acknowledgements

This research was supported by the Industrial Strategic Technology Development Program (20003968) funded by the Ministry of Trade, Industry & Energy (MOTIE, Korea). This research was supported by the National Research Foundation of Korea (NRF-2016M3D1A1027665 and NRF-2019R1A2C2084114) funded by Ministry of Science and ICT. In addition, this work was partially supported by the Brain Korea 21 PLUS project (Center for Creative Industrial Materials).

References

1 S. Gao, G. Liu, H. Yang, C. Hu, Q. Chen, G. Gong, W. Xue, X. Yi, J. Shang and R.-W. Li, *ACS Nano*, 2019, **13**, 2634–2642.
2 G. Wang, R. Wang, W. Kong and J. Zhang, *Cognit. Neurodyn.*, 2018, **12**, 615–624.
3 W. Deng, X. Zhang, R. Jia, L. Huang, X. Zhang and J. Jie, *NPG Asia Mater.*, 2019, **11**, 77.
4 Z. D. Luo, X. Xia, M. M. Yang, N. R. Wilson, A. Gruverman and M. Alexe, *ACS Nano*, 2020, **14**, 746–754.
5 S. Chen, Z. Lou, D. Chen and G. Shen, *Adv. Mater.*, 2018, **30**, 1705400.
6 C. Koch and B. Mathur, *IEEE Spectrum*, 1996, **33**, 38–46.
7 G. Indiveri and R. Douglas, *Science*, 2000, **288**, 1189–1190.
8 F. M. Ma, Y. B. Zhu, Z. W. Xu, Y. Liu, X. J. Zheng, S. Ju, Q. Q. Li, Z. Q. Ni, H. L. Hu, Y. Chai, C. X. Wu, T. W. Kim and F. S. Li, *Adv. Funct. Mater.*, 2020, **30**, 1908901.
9 H. L. Park, H. Kim, D. Lim, H. Zhou, Y. H. Kim, Y. Lee, S. Park and T. W. Lee, *Adv. Mater.*, 2020, **32**, 1906899.
10 Y. Wang, J. Yang, Z. Wang, J. Chen, Q. Yang, Z. Lv, Y. Zhou, Y. Zhai, Z. Li and S. T. Han, *Small*, 2019, **15**, 1805431.
11 M.-K. Kim and J.-S. Lee, *Adv. Mater.*, 2020, **32**, 1907826.
12 B. Pradhan, S. Das, J. Li, F. Chowdhury, J. Cherusseri, D. Pandey, D. Dev, A. Krishnaprasad, E. Barrios, A. Towers, A. Gesquiere, L. Tetard, T. Roy and J. Thomas, *Sci. Adv.*, 2020, **6**, eaay5225.
13 L. Yin, W. Huang, R. Xiao, W. Peng, Y. Zhu, Y. Zhang, X. Pi and D. Yang, *Nano Lett.*, 2020, **20**, 3378–3387.
14 K. Wang, S. Dai, Y. Zhao, Y. Wang, C. Liu and J. Huang, *Small*, 2019, **15**, 1900010.
15 L. Qian, Y. Sun, M. Wu, C. Li, D. Xie, L. Ding and G. Shi, *Nanoscale*, 2018, **10**, 6837–6843.
16 X. Zhu and W. D. Lu, *ACS Nano*, 2018, **12**, 1242–1249.
17 S. Ham, S. Choi, H. Cho, S.-I. Na and G. Wang, *Adv. Funct. Mater.*, 2019, **29**, 1806646.
18 Y. Wang, Z. Lv, J. Chen, Z. Wang, Y. Zhou, L. Zhou, X. Chen and S. T. Han, *Adv. Mater.*, 2018, **30**, 1802883.
19 Q. Wang, B. Chen, Y. Liu, Y. Deng, Y. Bai, Q. Dong and J. Huang, *Energy Environ. Sci.*, 2017, **10**, 516–522.
20 B. Li, Y. Li, C. Zheng, D. Gao and W. Huang, *RSC Adv.*, 2016, **6**, 38079–38091.
21 B. Hwang and J.-S. Lee, *Adv. Opt. Mater.*, 2019, **7**, 1801356.
22 H. Lin, C. Zhou, Y. Tian, T. Siegrist and B. Ma, *ACS Energy Lett.*, 2018, **3**, 54–62.
23 S. Chen and G. Shi, *Adv. Mater.*, 2017, **29**, 1605448.
24 K. Hong, Q. V. Le, S. Y. Kim and H. W. Jang, *J. Mater. Chem. C*, 2018, **6**, 2189–2209.
25 Y. Liao, H. Liu, W. Zhou, D. Yang, Y. Shang, Z. Shi, B. Li, X. Jiang, L. Zhang, L. N. Quan, R. Quintero-Bermudez, B. R. Sutherland, Q. Mi, E. H. Sargent and Z. Ning, *J. Am. Chem. Soc.*, 2017, **139**, 6693–6699.
26 J. Zhou, Y. Chu and J. Huang, *ACS Appl. Mater. Interfaces*, 2016, **8**, 25660–25666.
27 F. Li, C. Ma, H. Wang, W. Hu, W. Yu, A. D. Sheikh and T. Wu, *Nat. Commun.*, 2015, **6**, 8238.
28 S. Chen, C. Teng, M. Zhang, Y. Li, D. Xie and G. Shi, *Adv. Mater.*, 2016, **28**, 5969–5974.
29 J.-Y. Chen, Y.-C. Chiu, Y.-T. Li, C.-C. Chueh and W.-C. Chen, *Adv. Mater.*, 2017, **29**, 1702217.
30 S. Yu, *Proc. IEEE*, 2018, **106**, 260–285.
31 A. Melianas, T. J. Quill, G. LeCroy, Y. Tuchman, H. V. Loo, S. T. Keene, A. Giovannitti, H. R. Lee, I. P. Maria, I. McCulloch and A. Salleo, *Sci. Adv.*, 2020, **6**, eabb2958.
32 X. W. Feng, X. K. Liu and K. W. Ang, *Nanophotonics*, 2020, **9**, 1579–1599.
33 D. Lee, B. Hwang and J.-S. Lee, *ACS Appl. Mater. Interfaces*, 2019, **11**, 20225–20231.
34 B. Hwang and J.-S. Lee, *Adv. Mater.*, 2017, **29**, 1701048.
35 L. K. Ono, M. R. Leyden, S. Wang and Y. Qi, *J. Mater. Chem. A*, 2016, **4**, 6693–6713.
36 A. Biswas, R. Bakthavatsalam and J. Kundu, *Chem. Mater.*, 2017, **29**, 7816–7825.
37 R. Azmi, N. Nurrosyid, S.-H. Lee, M. Al Mubarok, W. Lee, S. Hwang, W. Yin, T. K. Ahn, T.-W. Kim, D. Y. Ryu, Y. R. Do and S.-Y. Jang, *ACS Energy Lett.*, 2020, **5**, 1396–1403.
38 Z. Yu, Z. Yang, Z. Ni, Y. Shao, B. Chen, Y. Lin, H. Wei, Z. J. Yu, Z. Holman and J. Huang, *Nat. Energy*, 2020, **5**, 657–665.
39 Z. Ni, C. Bao, Y. Liu, Q. Jiang, W.-Q. Wu, S. Chen, X. Dai, B. Chen, B. Hartweg, Z. Yu, Z. Holman and J. Huang, *Science*, 2020, **367**, 1352–1358.
40 Y. Chen, N. Li, L. Wang, L. Li, Z. Xu, H. Jiao, P. Liu, C. Zhu, H. Zai, M. Sun, W. Zou, S. Zhang, G. Xing, X. Liu, J. Wang, D. Li, B. Huang, Q. Chen and H. Zhou, *Nat. Commun.*, 2019, **10**, 1112.
41 A. Fakharuddin, W. Qiu, G. Croes, A. Devižis, R. Gegevičius, A. Vakhnin, C. Rolin, J. Genoe, R. Gehlhaar, A. Kadashchuk, V. Gulbinas and P. Heremans, *Adv. Funct. Mater.*, 2019, **29**, 1904101.
42 N. Liu, P. Liu, H. Zhou, Y. Bai and Q. Chen, *J. Phys. Chem. Lett.*, 2020, **11**, 3521–3528.
43 J. Haruyama, K. Sodeyama, L. Han and Y. Tateyama, *J. Am. Chem. Soc.*, 2015, **137**, 10048–10051.
44 S. Meloni, T. Moehl, W. Tress, M. Franckevičius, M. Saliba, Y. H. Lee, P. Gao, M. K. Nazeeruddin, S. M. Zakeeruddin, U. Rothlisberger and M. Graetzel, *Nat. Commun.*, 2016, **7**, 10334.

Published on 05 2021. Downloaded on 31.01.2026 06:16:23.

45 B. Hwang, C. Gu, D. Lee and J.-S. Lee, *Sci. Rep.*, 2017, **7**, 43794.
46 Y. Lin, Y. Bai, Y. Fang, Q. Wang, Y. Deng and J. Huang, *ACS Energy Lett.*, 2017, **2**, 1571–1572.
47 X. Xiao, J. Dai, Y. Fang, J. Zhao, X. Zheng, S. Tang, P. N. Rudd, X. C. Zeng and J. Huang, *ACS Energy Lett.*, 2018, **3**, 684–688.
48 W. Xu, H. Cho, Y. H. Kim, Y. T. Kim, C. Wolf, C. G. Park and T. W. Lee, *Adv. Mater.*, 2016, **28**, 5916–5922.
49 B. Chen, M. Yang, S. Priya and K. Zhu, *J. Phys. Chem. Lett.*, 2016, **7**, 905–917.
50 S. Wei, F. Wang, X. Zou, L. Wang, C. Liu, X. Liu, W. Hu, Z. Fan, J. C. Ho and L. Liao, *Adv. Mater.*, 2020, **32**, 1907527.
51 C. Xie and F. Yan, *J. Mater. Chem. C*, 2018, **6**, 1338–1342.
52 C. Xie, P. You, Z. Liu, L. Li and F. Yan, *Light: Sci. Appl.*, 2017, **6**, e17023.
53 Y. Liu, H. Wei, J. Guo, P.-A. Chen, S. Liu, J. Li, L. Miao, N. Wang, Z. Chen, J. Wang, H. Chen and Y. Hu, *Org. Electron.*, 2019, **75**, 105372.
54 E. R. Kandel, *Science*, 2001, **294**, 1030–1038.
55 S. J. Martin, P. D. Grimwood and R. G. M. Morris, *Annu. Rev. Neurosci.*, 2000, **23**, 649–711.
56 L. F. Abbott and S. B. Nelson, *Nat. Neurosci.*, 2000, **3**, 1178–1183.
57 J. L. McGaugh, *Science*, 2000, **287**, 248–251.
58 T. Ohno, T. Hasegawa, T. Tsuruoka, K. Terabe, J. K. Gimzewski and M. Aono, *Nat. Mater.*, 2011, **10**, 591–595.
59 R. S. Zucker and W. G. Regehr, *Annu. Rev. Physiol.*, 2002, **64**, 355–405.
60 Y. H. Liu, L. Q. Zhu, P. Feng, Y. Shi and Q. Wan, *Adv. Mater.*, 2015, **27**, 5599–5604.
61 C. S. Yang, D. S. Shang, N. Liu, G. Shi, X. Shen, R. C. Yu, Y. Q. Li and Y. Sun, *Adv. Mater.*, 2017, **29**, 1700906.
62 L. Yin, C. Han, Q. Zhang, Z. Ni, S. Zhao, K. Wang, D. Li, M. Xu, H. Wu, X. Pi and D. Yang, *Nano Energy*, 2019, **63**, 103859.
63 Y. Sun, L. Qian, D. Xie, Y. Lin, M. Sun, W. Li, L. Ding, T. Ren and T. Palacios, *Adv. Funct. Mater.*, 2019, **29**, 1902538.
64 S. Choi, S. H. Tan, Z. Li, Y. Kim, C. Choi, P. Y. Chen, H. Yeon, S. Yu and J. Kim, *Nat. Mater.*, 2018, **17**, 335–340.
65 S. Ambrogio, P. Narayanan, H. Tsai, R. M. Shelby, I. Boybat, C. di Nolfo, S. Sidler, M. Giordano, M. Bodini, N. C. P. Farinha, B. Killeen, C. Cheng, Y. Jaoudi and G. W. Burr, *Nature*, 2018, **558**, 60–67.
66 M. K. Kim and J.-S. Lee, *Nano Lett.*, 2019, **19**, 2044–2050.

 This journal is © The Royal Society of Chemistry 2021